Anharmonic Vibrational States of Solids from DFT Calculations. Part I: Description of the Potential Energy Surface

Alessandro Erba,*[†] Jefferson Maul,[†] Matteo Ferrabone,[†] Philippe Carbonnière,[‡] Michel Rérat,[‡] and Roberto Dovesi[†]

[†]Dipartimento di Chimica, Universitá di Torino, via Giuria 5, 10125 Torino, Italy

[‡]IPREM, Université de Pau et des Pays de l'Adour, IPREM-CAPT UMR CNRS 5254, Hélioparc Pau Pyrénées, 2 avenue du Président Angot, 64053 PAU CEDEX 9, Pau, France

ABSTRACT: A computational approach is presented to compute anharmonic vibrational states of solids from quantum-mechanical DFT calculations by taking into explicit account phonon−phonon couplings via the vibrational configuration interaction (VCI) method. The Born−Oppenheimer potential energy surface (PES) is expanded in a Taylor's series in terms of harmonic normal coordinates, centered at the equilibrium nuclear configuration, is truncated to quartic order, and contains one-mode, two-mode, and three-mode interatomic force constants. The description of the anharmonic terms of the PES involves the numerical evaluation of high-order energy derivatives (cubic and quartic

in our case) with respect to nuclear displacements and constitutes the most computationally demanding step in the characterization of anharmonic vibrational states of materials. Part I is devoted to the description of the PES. Four different numerical approaches are presented for the description of the potential, all based on a grid representation of the PES in the basis of the normal coordinates, that require different ingredients (energy and/or forces) to be evaluated at each point (i.e., nuclear configuration) of the grid. The numerical stability and relative computational efficiency of the various schemes for the description of the PES are discussed on two molecular systems (water and methane) and two extended solids (Ice-XI and MgH_2). All the presented algorithms are implemented into a developmental version of the Crystal program.
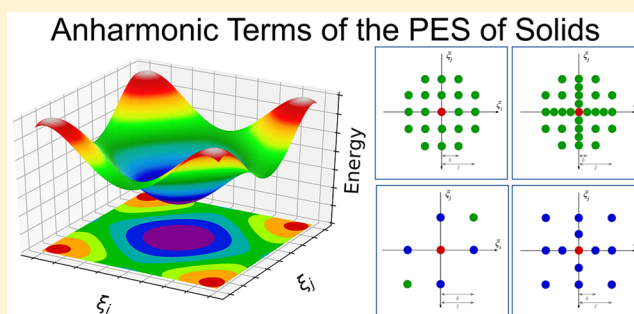
I. INTRODUCTION

Atomic vibrations are involved in a variety of thermal properties of finite molecular systems and extended solids. In particular, thermal properties of materials (such as specific heat, entropy, thermal expansion, thermo-elasticity, lattice thermal conductivity, etc.) are strictly connected to the lattice dynamics of the system.[1] Statistical thermodynamics provides the link between the microscopic atomistic description of the nuclear dynamics (i.e., the quantum-mechanical vibrational states) and macroscopic thermal properties of matter.[2]

The energy of vibrational states of molecules can be effectively probed with vibrational spectroscopies such as infrared and Raman. The same techniques are used to probe those lattice vibrations of solids where atoms of different lattice cells move in phase with each other (i.e., phonons at the Γ point of the Brillouin zone).[3] Inelastic neutron scattering can be used to probe also out-of-phase vibrations (i.e., the so-called phonon dispersion).[4]

In the context of standard quantum-mechanical simulations of materials, the usual way in which the lattice dynamics of the system is described is by means of the harmonic approximation (HA) of the Born−Oppenheimer potential energy surface (PES).[5] The HA assumes a quadratic form of the Taylor's expansion of the PES in terms of atomic displacements from the

equilibrium configuration and implies a description of the lattice dynamics in terms of a set of independent quantum harmonic oscillators. Despite its simplicity, the HA has experienced great success in the description of lattice vibrations of many classes of materials,[6−11] in particular those without light elements (mainly hydrogen)[12,13] and without strongly anharmonic phonon modes, such as ferroelectric ABO_3 perovskites, for instance.[14−17]

At the same time, the limitations of the HA are well known and, in a solid state context, can be grouped into two classes: (i) the constant-volume nature of all computed thermal properties of materials and (ii) the neglected high-order terms of the PES, which result in the independence of phonon modes. The first class of limitations is such that the HA is unable to describe the thermal lattice expansion of the system, as well as its thermo-elasticity (i.e., thermal dependence of the mechanical response). Furthermore, at the harmonic level, there is no distinction between constant-volume and constant-pressure thermodynamic functions (such as the specific heat, for instance). These limitations can be effectively overcome by using the so-called quasi-harmonic approximation (QHA), which requires the evaluation of harmonic phonon frequencies as a function of

lattice cell volume.[18,19] Some of the authors of this paper have recently developed a fully automated module for the calculation of quasi-harmonic thermal properties of materials in the CRYSTAL program.[20−26] The second type of limitations is due to neglected higher-than-second-order terms in the expansion of the PES, so that the intrinsic anharmonicity of the phonon modes as well as phonon−phonon couplings—and their effects on vibrational states (such as Darling−Dennison and Fermi resonances and phonon combination bands)—are in turn neglected, which results in the approximated description of thermodynamic properties.[27,28] As a further consequence of the lack of cubic terms of the PES within the HA, phonon lifetimes τ would be infinite as well as the lattice thermal conductivity of the material.

While several schemes have been developed in the last years to determine the cubic interatomic force constants needed to compute the lattice thermal conductivity,[29−34] less effort has been put in the characterization of the PES up to fourth order and in the corresponding description of anharmonic vibrational states of solids by taking full account of phonon−phonon couplings. In this respect, a few notable exceptions are represented by (i) the self-consistent phonon theory (SCPH)[35] as implemented by Tadano,[36,37] where relevant cubic and quartic terms of the PES are selected through compressive sensing[38] (ii) the vibrational self-consistent field (VSCF) approach[39] as implemented for solids by Monserrat et al.,[40,41] where one- and two-mode terms of the PES are obtained from fitting the energy computed in rich 1D and 2D grids of nuclear configurations (only recently, analytical forces have been used to improve the numerical stability and efficiency of the fitting procedure of the PES, see ref 42), (iii) the self-consistent *ab initio* lattice dynamics (SCAILD) method,[43] (iv) the stochastic self-consistent harmonic approximation (SSCHA),[44] and (v) Parlinski's modified version of the previous two approaches.[45] Most of the above-mentioned anharmonic approaches take into account phonon−phonon couplings within a mean-field approach.

In this two-part paper, we present the first implementation of the vibrational configuration interaction (VCI) method—based or not on a reference VSCF solution—to determine anharmonic vibrational states of solids by taking phonon−phonon interactions into full account. In a molecular context, a hierarchy of well-assessed methodologies exists for treating mode−mode couplings, which reflects the hierarchy of methodologies used in the description of dynamic electron correlation in electronic structure theory:[46,47] the VSCF approach,[39] where vibration modes interact through a mean-field potential; vibrational perturbation theory truncated at the nth order (VPTn), where the reference state is given by VSCF;[48,49] the vibrational coupled-cluster approach (VCC)[50] and VCI, where mode−mode couplings are treated exactly (at least in the full-VCI limit).[51−57]

In Part I, we discuss the expansion of the PES of a solid in terms of its harmonic normal modes, and we illustrate four different methods to compute its high-order anharmonic terms. The numerical description of the PES from static density functional theory (DFT) calculations indeed represents the most delicate and computationally expensive step in the anharmonic treatment of vibrational states of materials. In this study, the PES is truncated to quartic order and contains one-, two-, and three-mode interatomic force constants. Different numerical approaches are presented, all based on a grid representation of the PES in the basis of the normal coordinates, that require different ingredients (energy and/or forces) to be evaluated at each point (i.e., nuclear configuration) of the grid. Different algorithms are explored to compute the high-order energy derivatives: energy fitting and finite differences. The numerical stability and relative computational efficiency of the various schemes is discussed on two molecular systems (water and methane) and two extended solids (Ice-XI and MgH_2).

In Part II,[58] we illustrate formal aspects of the VSCF and VCI methods, and we present their implementation for solids. The correctness of the implementation is documented through comparison of available computational and experimental results. The convergence of the configuration-interaction expansion is explicitly discussed, and theoretical approaches to improve its convergence illustrated. Furthermore, the effect of the exchange-correlation functional of the DFT and the basis set used in the description of the PES on the computed anharmonic vibrational states of molecules and solids is explicitly discussed. All the presented algorithms have been implemented into a developmental version of the CRYSTAL17 program.[59,60]

II. FORMAL ASPECTS

In the following, we discuss some formal aspects of vibrational states of molecules and solids, where, in the case of solids, we restrict our attention to Γ-point vibration modes. However, let us note that, by working in terms of a supercell of the primitive one, vibration modes of solids proper of different **k**-points can be folded back to the Γ-point. The starting point of our anharmonic vibrational description is represented by the harmonic approximation according to which the nuclear dynamics of the system is described in terms of a set of M independent quantum harmonic oscillators, whose corresponding normal coordinates are $Q_1, Q_2, \cdots, Q_M \equiv \mathbf{Q}$.

Within the Born−Oppenheimer approximation, vibrational states are determined by solving the nuclear Schrödinger equation, which, in terms of normal coordinates, reads

$$\mathcal{H}\Psi_s(\mathbf{Q}) = E_s\Psi_s(\mathbf{Q}) \tag{1}$$

where $\Psi_s(\mathbf{Q})$ is the vibrational wave function of the sth vibrational state and E_s the corresponding energy. By setting the rotational angular momentum to zero and by neglecting rotational coupling effects, the Hamiltonian operator in eq 1 can be written as

$$\mathcal{H} = \sum_{i=1}^{M} -\frac{1}{2}\frac{\partial^2}{\partial Q_i^2} + V(\mathbf{Q}) \tag{2}$$

where $V(\mathbf{Q})$ is the usual Born−Oppenheimer potential energy surface (PES) in the basis of mass-weighted normal coordinates. As discussed in the Introduction, the description of the potential term in the Hamiltonian above is a computationally challenging task. Here, we expand the PES in a Taylor's series centered at the equilibrium nuclear configuration as follows:

$$\begin{aligned}
V(\mathbf{Q}) = \frac{1}{2}\sum_{i=1}^{M}\omega_i^2 Q_i^2 &+ \frac{1}{3!}\sum_{i,j,k=1}^{M}\eta_{ijk}Q_iQ_jQ_k \\
&+ \frac{1}{4!}\sum_{i,j,k,l=1}^{M}\eta_{ijkl}Q_iQ_jQ_kQ_l \\
&+ \frac{1}{5!}\sum_{i,j,k,l,m=1}^{M}\eta_{ijklm}Q_iQ_jQ_kQ_lQ_m + \cdots
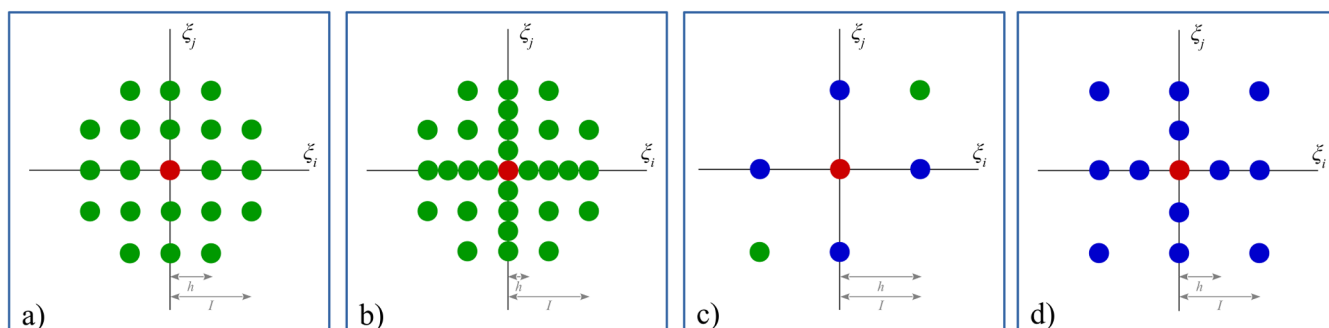\end{aligned} \tag{3}$$

Figure 1. 2D grid of points defining the nuclear configurations that need to be considered in the evaluation of the adiabatic PES in its 2M4T representation for the four different schemes discussed in Section IIB: (a) energy finite differences (Scheme 1), (b) energy fit (Scheme 2), (c) EGH finite differences, two points (Scheme 3), and (d) EGH finite differences, four points (Scheme 4). Different colors correspond to different quantities computed for each nuclear configuration: only energy (green), energy and forces (blue), and energy, forces, and Hessian (red). The axes are in units of frequency-scaled normal coordinates: $\xi_i \propto Q_i \sqrt{\omega_i}$.

where ω_i is the harmonic frequency of the ith vibration normal mode and where η_{ijk}, η_{ijkl}, and η_{ijklm} are cubic, quartic, and fifth-order force constants, respectively

$$\eta_{ijk} = \left(\frac{\partial^3 E}{\partial Q_i \partial Q_j \partial Q_k} \right) \tag{4}$$

$$\eta_{ijkl} = \left(\frac{\partial^4 E}{\partial Q_i \partial Q_j \partial Q_k \partial Q_l} \right) \tag{5}$$

$$\eta_{ijklm} = \left(\frac{\partial^5 E}{\partial Q_i \partial Q_j \partial Q_k \partial Q_l \partial Q_m} \right) \tag{6}$$

The inclusion of anharmonic (i.e., higher than quadratic) terms in the potential (eq 3) therefore implies the evaluation of high-order energy derivatives with respect to atomic displacements. These high-order energy derivatives have to be computed numerically, which makes the description of the PES a computationally demanding task. For this reason, it proves crucial to devise (i) effective strategies to truncate the expansion of the PES in eq 3 so as to include only those terms contributing significantly to the description of the vibrational states of the system and (ii) efficient algorithms for the numerical evaluation of the high-order energy derivatives in eqs 4−6. We discuss details of both aspects below.

IIA. Truncation of the PES. When working in terms of a Taylor expansion of the potential of the type given in eq 3, it is a common practice in molecular anharmonic calculations to truncate it after the fourth order as in most cases neglected higher-order terms would produce little corrections to the vibrational states, and at the same time, they would lead to a dramatic increase in the computational cost (higher than fourth-order terms are however needed in some strongly anharmonic systems).[61] Here, we adopt the same strategy, and thus, we include only terms up to fourth order in the PES (namely, we use a 4T representation of the potential). Within a 4T representation, the PES can be further truncated by considering only those force constants involving a maximum of n distinct modes (namely, a nM representation of the potential). By combining the two truncation strategies introduced above, a 1M4T representation of the PES would require the evaluation of the next force constants

$$\eta_{iii}, \eta_{iiii} \quad \forall\ i \in M \tag{7}$$

This representation of the PES neglects two-mode couplings and almost always results in a wrong description of the vibrational states. A popular representation of the potential is the 2M4T one, which includes all two-mode coupling force constants

$$\eta_{iii}, \eta_{iiii} \quad \forall\ i \in M$$
$$\eta_{ijj}, \eta_{iij}, \eta_{iiij}, \eta_{ijjj}, \eta_{iijj} \quad \forall\ i < j \in M \tag{8}$$

Analogously, the 3M4T representation of the PES includes the following terms:

$$\eta_{iii}, \eta_{iiii} \quad \forall\ i \in M$$
$$\eta_{ijj}, \eta_{iij}, \eta_{iiij}, \eta_{ijjj}, \eta_{iijj} \quad \forall\ i < j \in M$$
$$\eta_{ijk}, \eta_{iijk} \quad \forall\ i < j < k \in M \tag{9}$$

Here, we work in terms of 2M4T and 3M4T representations of the PES as given in eqs 8 and 9, respectively. We have implemented into the CRYSTAL program four different algorithms to describe the 2M4T potential and two different algorithms to describe the 3M4T potential, which we illustrate below.

IIB. Numerical Evaluation of High-Order Force Constants. The cubic and quartic force constants entering the expansion of the PES discussed in Section IIA have to be evaluated numerically. Two different approaches can be used in this respect (fitting and finite differences), which both require the evaluation of the energy (and forces) on a grid of points (i.e., displaced atomic configurations). The numerical evaluation of such high-order energy derivatives is a rather delicate computational task, whose stability with respect to the adopted grid of points has to be carefully addressed. In particular, the numerical stability of the description has to be discussed in terms of number of points, interval explored, and type of ingredients available at each point (energy alone or energy and forces).

We have developed and implemented four different numerical approaches to compute those terms of the PES required to get a 2M4T representation, which we discuss in detail below. Different approaches are characterized by a different numerical stability, accuracy, and computational cost. All these aspects are addressed in this paper. In order to get two-mode terms, for each pair of modes (Q_i, Q_j), a grid of points is needed where the

energies (and forces, for some approaches) are computed. The shape of this grid is illustrated in Figure 1 for the four different schemes that we describe. The first two schemes only require the evaluation of the energy at each displaced nuclear configuration, while the last two combine information from the energy and forces.

IIB1. Scheme 1: Energy Finite Differences. In this scheme, originally proposed by Lin et al.,[61] all the terms of the PES in eq 8 are obtained from finite differences of the energy computed on the grid illustrated in Figure 1a. For each pair of modes (Q_i, Q_j), the corresponding cubic and quartic force constants are obtained from the following expressions:

$$\eta_{iii} = \frac{1}{2s_i^3}(-E_{-2} + 2E_{-1} - 2E_1 + E_2) \tag{10}$$

$$\eta_{iij} = \frac{1}{2s_i^2 s_j}(2E_{0,-1} - 2E_{0,1} - E_{-1,-1} + E_{-1,1} - E_{1,-1} + E_{1,1}) \tag{11}$$

$$\eta_{iiii} = \frac{1}{s_i^4}(6E_0 + E_{-2} - 4E_{-1} - 4E_1 + E_2) \tag{12}$$

$$\eta_{iiij} = \frac{1}{4s_i^3 s_j}(E_{-2,-1} - E_{-2,1} - 2E_{-1,-1} + 2E_{-1,1} + 2E_{1,-1} - 2E_{1,1} - E_{2,-1} + E_{2,1}) \tag{13}$$

$$\eta_{iijj} = \frac{1}{s_i^2 s_j^2}(4E_{0,0} - 2E_{0,-1} - 2E_{0,1} - 2E_{-1,0} + E_{-1,-1} - E_{-1,1} - 2E_{1,0} + E_{1,-1} + E_{1,1}) \tag{14}$$

where $s_i = h/\sqrt{\omega_i}$ and $s_j = h/\sqrt{\omega_j}$ are the adaptive steps among the points of the grid along the Q_i and Q_j normal coordinates (see below for more details on how the h step is defined) and where $E_{a,b}$ is the energy computed at a nuclear configuration displaced by $as_iQ_i + bs_jQ_j$ from the equilibrium one. For those terms of the PES involving only one mode, a more compact notation is used where E_a is the energy of a nuclear configuration displaced by as_iQ_i from the equilibrium one. For a system with M normal modes, the total number of points to be considered in the definition of the PES with this scheme is given by

$$N_{\text{scheme1}} = 1 + 4M + 12\binom{M}{2} \tag{15}$$

where "1" is the equilibrium configuration on which the Hessian is evaluated to get the harmonic vibration modes, $4M$ are those nuclear configurations that are obtained by displacing the atoms only along one normal coordinate, and the last term counts the number of nuclear configurations obtained by displacing atoms along two normal coordinates. In particular, the binomial factor in eq 15 counts the number of independent pairs of modes within the set of M modes, and 12 is the number of displaced points per pair.

IIB2. Scheme 2: Energy Fit. Also, this scheme, as the previous one, requires only the energy to be evaluated at the different nuclear configurations explored. The grid of points used within this scheme is sketched in Figure 1b. This scheme consists of computing the energy on the grid and then in best-fitting those values to the function below

$$E(Q_i, Q_j) = c_1 Q_i + c_2 Q_j + c_3 Q_i^2 + c_4 Q_j^2 + c_5 Q_i Q_j$$
$$+ c_6 Q_i^3 + c_7 Q_j^3 + c_8 Q_i^2 Q_j + c_9 Q_i Q_j^2 + c_{10} Q_i^4 + c_{11} Q_j^4$$
$$+ c_{12} Q_i^3 Q_j + c_{13} Q_i Q_j^3 + c_{14} Q_i^2 Q_j^2 + c_{15} Q_i^5 + c_{16} Q_j^5 \tag{16}$$

All the terms of the 2M4T representation of the PES in eq 8 can thus be obtained from the coefficients above as

$$\eta_{iii} = 6c_7, \; \eta_{iij} = 2c_8, \; \eta_{iiii} = 24c_{10}, \; \eta_{iiij} = 6c_{12}, \; \eta_{iijj} = 4c_{14} \tag{17}$$

Let us stress that, in principle, the c_1 and c_2 coefficients should be null as they correspond to the forces acting on the atoms at the equilibrium configuration. Moreover, the c_5 coefficient should also vanish because it represents a mixed second energy derivative in the basis of the normal modes (where the Hessian takes a diagonal form). By deleting the corresponding terms in the function (eq 16), constraints on the forces and Hessian would be applied. Here, we prefer to keep those terms so as to cope with possible small numerical inaccuracies in the geometry optimization process. For a system with M normal modes, the total number of nuclear configurations to be considered in the definition of the PES with this scheme is given by

$$N_{\text{scheme2}} = 1 + 8M + 12\binom{M}{2} \tag{18}$$

IIB3. Scheme 3: EGH Finite Differences (Two Points). In order to further reduce the number of points in the grid to be explicitly explored, one has to introduce some additional information at some of the nuclear configurations. By computing the analytical gradients at some configurations (only those where atoms are displaced along one normal coordinate at a time), an effective finite difference scheme has been devised,[61] which is called EGH from the different ingredients it requires: energy, gradients, and Hessian. Figure 1c shows the points needed for each pair of modes (Q_i, Q_j), where some nuclear configurations only require the energy to be evaluated while others require energy and gradients. The Hessian matrix is computed just at the equilibrium nuclear configuration to get the harmonic normal modes and frequencies. For each pair of modes, all the terms of the 2M4T representation of the PES in eq 8 can be obtained from the following finite difference relations:

$$\eta_{iii} = \frac{1}{s_i^2}(G_{-1}^i - 2G_0^i + G_1^i) \tag{19}$$

$$\eta_{iij} = \frac{1}{s_i^2}(G_{-1,0}^j - 2G_{0,0}^j + G_{1,0}^j) \tag{20}$$

$$\eta_{iiii} = \frac{3}{s_i^3}(G_1^i - 2s_i\omega_i - G_{-1}^i) \tag{21}$$

$$\eta_{iiij} = \frac{3}{s_i^3}(G_{1,0}^j - G_{-1,0}^j) \tag{22}$$

$$\eta_{iijj} = -\frac{1}{2s_i^2 s_j^2}(8E_{0,0} - 4E_{-1,-1} - 4E_{1,1} - s_j G_{0,-1}^j + s_j G_{0,1}^j$$
$$- s_i G_{-1,0}^i + s_i G_{1,0}^i - 4s_j G_{-1,0}^j + 4s_j G_{1,0}^j - 4s_j G_{0,-1}^i$$
$$+ 4s_i G_{0,1}^i + 2s_i^2 \omega_i + 2s_j^2 \omega_j) \tag{23}$$

where $E_{a,b}$ has the same meaning as above, and where $G^i_{a,b}$ is the gradient with respect to Q_i computed at a nuclear configuration displaced by $as_iQ_i + bs_jQ_j$ from the equilibrium one (analogously, $G^j_{a,b}$ is the gradient with respect to Q_j computed at the same nuclear configuration). For those terms of the PES involving only one mode, a more compact notation is used where G^i_a is the gradient with respect to Q_i of a nuclear configuration displaced by as_iQ_i from the equilibrium one.

In the expressions above to compute η_{iii} and η_{iij}, we use G^i_0 and $G^i_{0,0}$ that are the first energy derivatives with respect to Q_i and Q_j at the equilibrium nuclear configuration, respectively. In principle, these quantities should be null, but we still include them here in order to take into account possible small numerical inaccuracies in the geometry optimization process leading to the equilibrium configuration.

For a system with M normal modes, the total number of points to be considered in the definition of the PES with this scheme is therefore given by

$$N_{\text{scheme3}} = 1 + 2M + 2\binom{M}{2} \tag{24}$$

The number of points required with this scheme is as low as it gets. At the same time, $2M$ points are now characterized by a larger cost as the additional evaluation of the forces is required. However, as we discuss later, the additional cost of the forces at an already considered nuclear configuration is lower than that of a calculation of the energy on a new nuclear configuration, which makes this scheme particularly efficient computationally.

IIB4. Scheme 4: EGH Finite Differences (Four Points). Along the lines of the previous scheme, we have derived expressions to compute the different terms in the 2M4T potential from finite differences of energy and forces evaluated on a richer grid of points, as sketched in Figure 1d. This scheme requires the forces to be evaluated at all the considered nuclear configurations. By following the same conventions introduced for the previous scheme, the expressions are the following:

$$\eta_{iii} = \frac{1}{12s_i^2}(-30G^i_0 - G^i_2 - G^i_{-2} + 16G^i_1 + 16G^i_{-1}) \tag{25}$$

$$\eta_{iij} = \frac{1}{12s_i^2}[-30G^j_{0,0} - G^j_{2,0} - G^j_{-2,0} + 16(G^j_{1,0} + G^j_{-1,0})] \tag{26}$$

$$\eta_{iiii} = \frac{1}{2s_i^3}(G^i_2 - G^i_{-2} + 2G^i_{-1} + 2G^i_1) \tag{27}$$

$$\eta_{iiij} = \frac{1}{2s_i^3}(G^j_{2,0} - G^j_{-2,0} + 2G^j_{-1,0} - 2G^j_{1,0}) \tag{28}$$

$$\eta_{iijj} = \frac{1}{16s_i^2 s_j}(2G^i_{-2,0} - 2G^i_{2,0} - G^i_{-2,-2} + G^i_{2,-2} - G^i_{-2,2} + G^i_{2,2}) \tag{29}$$

Also, in this case, the first energy derivatives with respect to normal modes at the equilibrium configuration are explicitly used in the expressions 26 and 27 for the same reasons discussed above. This scheme is expected to ensure a higher numerical stability on the computed terms of the PES than the previous one (this is discussed in Section III) but at the same time is characterized by a computational cost that is about twice that of the previous one. Indeed, for a system with M modes, the

number of nuclear configurations to be explicitly explored is given by

$$N_{\text{scheme4}} = 1 + 4M + 4\binom{M}{2} \tag{30}$$

IIB5. 3M4T Representation of the PES. Here, we discuss how we can compute the additional terms of the PES needed to get a 3M4T representation, as given in eq 9, namely, η_{ijk} and η_{iijk}. It turns out that these three-mode terms can be evaluated quite effectively from EGH finite difference expressions. We show below how these three-mode terms of the PES can be computed from a slightly modified version of the Scheme 3 discussed above and from the Scheme 4 as such for the 2M4T representation.

By exploiting the information provided by the computed forces, both η_{ijk} and η_{iijk} can indeed be computed from the same set of nuclear configurations explored in the 2M4T description of the PES, without the need to explicitly explore nuclear configurations obtained by displacing atoms along three distinct modes. Figure 2 shows the 2D grid of points required for each pair of modes to get the three-mode terms with the two EGH schemes that we have implemented.
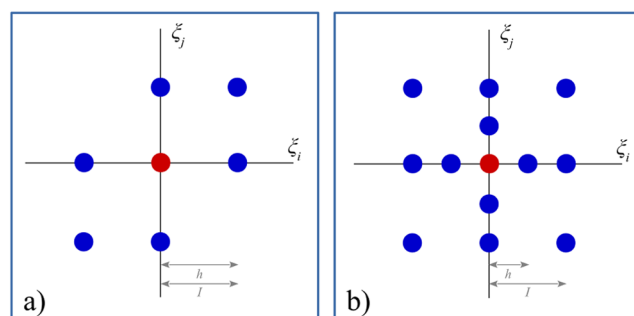

Figure 2. 2D grid of points defining the nuclear configurations that need to be considered in the evaluation of the adiabatic PES in its 3M4T representation for the two EGH schemes discussed in Section IIB: (a) EGH finite differences, two points (Scheme 3) and (b) EGH finite differences, four points (Scheme 4). Different colors correspond to different quantities computed for each nuclear configuration: energy and forces (blue) and energy, forces, and Hessian (red). The axes are in units of frequency-scaled normal coordinates: $\xi_i \propto Q_i\sqrt{\omega_i}$.

The comparison of panel (a) of Figure 2 with panel (c) of Figure 1 shows that, in order to get three-mode terms, Scheme 3 is modified in such a way to compute the forces also at mixed displaced configurations and not only at those obtained by displacing along only one normal coordinate. Once all the pairs of modes have been considered, and the corresponding nuclear configurations explored, with this approach (modified Scheme 3) the three-mode terms are evaluated as

$$\eta_{ijk} = \frac{1}{2s_i s_j}(2G^i_{0,0,0} - G^i_{0,0,-1} - G^i_{0,0,1} - G^i_{0,-1,0} + G^i_{0,-1,-1} - G^i_{0,1,0} + G^i_{0,1,1}) \tag{31}$$

$$\eta_{iijk} = \frac{1}{2s_i^2 s_j s_k}[(G_{-1,-1,0}^k - G_{-1,0,0}^k - G_{0,-1,0}^k + G_{0,1,0}^k$$
$$+ G_{1,0,0}^k - G_{1,1,0}^k)s_k + (G_{-1,0,-1}^j - G_{-1,0,0}^j - G_{0,0,-1}^j$$
$$+ G_{0,0,1}^j + G_{1,0,0}^j - G_{1,0,1}^j)s_j + (G_{0,-1,0}^i - G_{0,-1,-1}^i$$
$$+ G_{0,0,-1}^i - G_{0,0,1}^i - G_{0,1,0}^i + G_{0,1,1}^i)s_i] \tag{32}$$

where here $G_{a,b,c}^i$ is the gradient with respect to Q_i computed at a nuclear configuration displaced by $as_iQ_i + bs_jQ_j + cs_kQ_k$ from the equilibrium one. Note that, as anticipated above, there are no nuclear configurations to be explored where a, b, and c are all nonzero at the same time, so that we can still work in terms of 2D grids.

Three-mode terms of the PES can also be obtained from Scheme 4 discussed above for the 2M4T representation (Figure 2b and Figure 1d) coincide). Indeed, it turns out that, when working with the Scheme 4, the evaluation of the three-mode terms η_{ijk} and η_{iijk} can be seen as a zero-cost byproduct. Once all the pairs of modes have been considered, with this approach (Scheme 4) the three-mode terms are evaluated as

$$\eta_{ijk} = \frac{1}{8s_i s_j}(2G_{0,0,0}^i - G_{0,0,-2}^i - G_{0,0,2}^i - G_{0,-2,0}^i + G_{0,-2,-2}^i$$
$$- G_{0,2,0}^i + G_{0,2,2}^i) \tag{33}$$

$$\eta_{iijk} = \frac{1}{16s_i^2 s_j s_k}[(G_{-2,-2,0}^k - G_{-2,0,0}^k - G_{0,-2,0}^k + G_{0,2,0}^k$$
$$+ G_{2,0,0}^k - G_{2,2,0}^k)s_k + (G_{-2,0,-2}^j - G_{-2,0,0}^j - G_{0,0,-2}^j$$
$$+ G_{0,0,2}^j + G_{2,0,0}^j - G_{2,0,2}^j)s_j + (G_{0,-2,0}^i - G_{0,-2,-2}^i$$
$$+ G_{0,0,-2}^i - G_{0,0,2}^i - G_{0,2,0}^i + G_{0,2,2}^i)s_i] \tag{34}$$

We discuss the computational cost of these different schemes in Section IIB7 below.

IIB6. Step Size. The accuracy of the finite difference expressions used for Schemes 1, 3, and 4 above clearly depends on the step size h used in the definition of the corresponding 2D grid of points. Similarly, the accuracy of energy-fitting Scheme 2 depends on the amplitude of the explored interval in the definition of the grid. We discuss the numerical stability of the different schemes with respect to the value of the step size h in Section III. Here, we discuss the type of step size that we use. In principle, two different strategies can be used: (i) a fixed step size for all modes and (ii) an adaptive step size based on the curvature of the PES at the equilibrium configuration. We refer to the comprehensive review by Lin et al. for an overview of the many different proposals in this respect, in a molecular context.[61] In a solid state context, the use of a fixed step size might become problematic as it can probe very unbalanced energy changes along vibration modes characterized by very different vibration frequencies. In solids, vibration frequencies typically span 3 orders of magnitude, from a few tens of cm^{-1} to a few thousands of cm^{-1}. Adaptive, mode-specific steps therefore represent the best choice to ensure a balanced description of high-order terms of the PES.

In our implementation, we define the 2D grids presented in Figures 1 and 2 in terms of dimensionless harmonic frequency-scaled normal coordinates

$$\xi_i \propto Q_i\sqrt{\omega_i} \tag{35}$$

By definition, for each vibration mode, when ξ is equal to 1 the harmonic potential energy coincides with the fundamental vibration energy level of the harmonic oscillator. We refer to $\xi = \pm 1$ as to the "classical amplitude" of the harmonic oscillator. See Figure 3 for a graphical definition of this quantity. Here, we
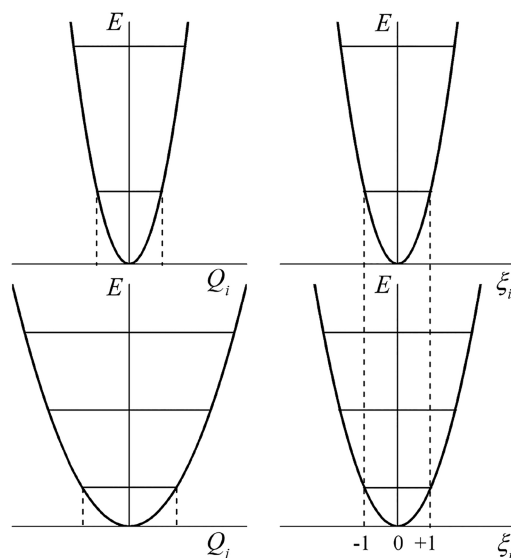

Figure 3. Two quantum harmonic oscillators as a function of the normal coordinates Q_i and Q_j (left panels) and as a function of the frequency-scaled coordinates ξ_i and ξ_j (right panels). When $\xi = \pm 1$, the harmonic potential energy equals the energy of the fundamental vibration state of the harmonic oscillator.

express the step size h and in general the explored interval of atomic displacements in units of ξ. As an example, by setting $h = 1$ for all modes, we would actually displace atoms differently along different normal modes. Along each normal mode, atoms would be displaced to such an extent to produce a change in the corresponding harmonic potential energy equal to the fundamental vibration energy level.

IIB7. Computational Cost of Different Schemes. We discuss the numerical stability of the different schemes introduced in the previous pages to describe high-order terms of the adiabatic PES in Section III. Here, we discuss their relative computational cost. The left panel of Figure 4 reports the total number of nuclear configurations that explicitly need to be explored in the construction of the PES (in the 2M4T and 3M4T representations) as a function of the number of vibration modes M one considers. The four lines correspond to the four numerical schemes introduced in Section IIB. The two lines corresponding to Scheme 1 and Scheme 2 look almost undistinguishable on the plot because, despite being characterized by a different number of points for single-mode configurations (4 versus 8, respectively), they require the same number of points for two-mode configurations (12 per pair of modes). The latter clearly dominate the scaling of the total number of configurations as a function of M because of the binomial factors in eqs 15 and 18. The two EGH methods, Scheme 3 and Scheme 4, require a much smaller number of nuclear configurations and are characterized by a much more favorable scaling with M because of the smaller prefactor (2 and 4, respectively) of the binomial term in eqs 24 and 30. In particular, Scheme 3 requires a number of configurations that is exactly half of that of Scheme 4.
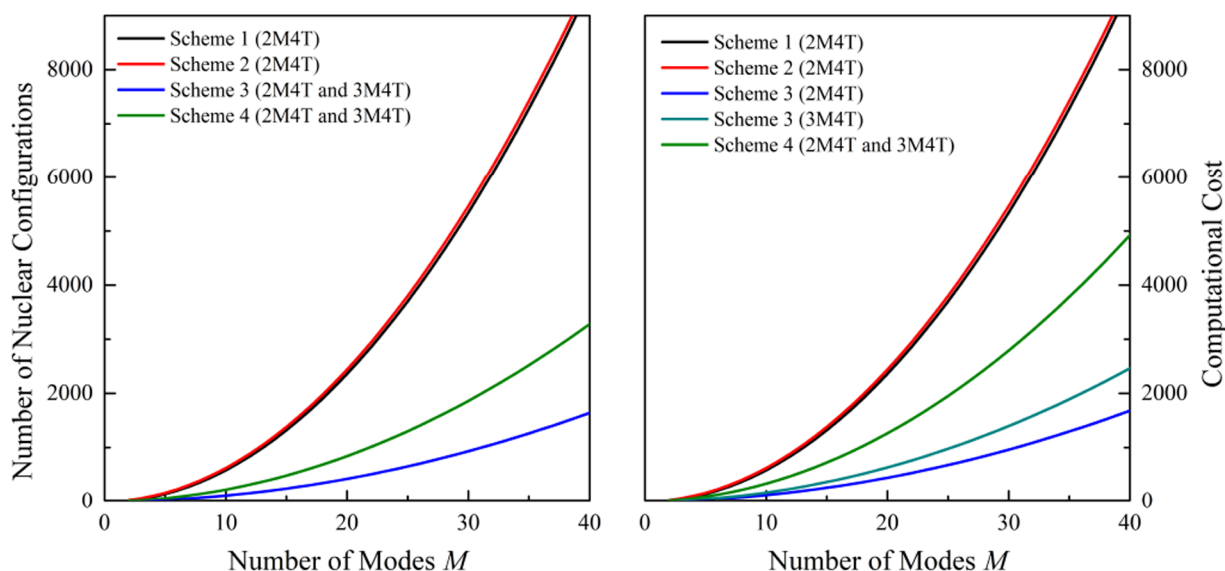
Figure 4. (Left) Total number of nuclear configurations to be explored in the construction of the PES (in the 2M4T and 3M4T representations) as a function of the number of vibration modes M of the system. The four lines correspond to the four numerical schemes introduced in Section IIB. (Right) Computational cost of the different schemes for the description of the PES as a function of M; the cost is normalized to that of a single-point SCF calculation (i.e., the cost of one SCF calculation is set to 1).

In the different methods, not all nuclear configurations are characterized by the same computational cost (note that here by computational cost we mainly refer to the time needed to perform the calculation). This is due to the fact that, depending on the adopted scheme, some configurations require only the evaluation of the energy (i.e., the solution of the SCF procedure), while others require the additional evaluation of the analytical forces. Depending on the particular system one studies, the evaluation of the forces can have a different cost relative to the SCF (see discussion in Section III). Here, we consider the worst case scenario in which the evaluation of the forces takes as much as 50% of the time needed to complete the SCF and compute the energy (in Section III, we show that much lower factors, down to 20%, are obtained for many small molecular systems). Within this assumption, the right panel of Figure 4 reports the computational cost of the different schemes for the description of the PES as a function of M. The cost is normalized to that of a single-point SCF calculation (i.e., the cost of one SCF calculation is set to 1). We clearly see that Scheme 3 (without and with inclusion of three-mode terms) is by far the most computationally efficient, implying a much lower computational cost than Scheme 4 (by a factor of about 2) and Schemes 1 and 2 (by a factor of about 5). From this preliminary analysis on the computational cost of the different schemes, Scheme 3 clearly represents the ideal choice. In Section III, we discuss the numerical stability and accuracy of the various schemes in order to check whether or not Scheme 3 can be safely used as a default choice in the mapping of the adiabatic PES.

III. NUMERICAL ASPECTS

An essential prerequisite to the reliable description of anharmonic vibrational states in molecular and periodic systems is the availability of accurate and stable numerical approaches for the evaluation of high-order terms in the expansion of the adiabatic PES in eq 3. The stability and relative performance of the different numerical schemes illustrated in Section IIB for the description of the PES are discussed below. In particular, we investigate the following: (i) How much is each numerical

scheme stable with respect to the investigated range of atomic displacements used in the definition of the 2D grids of points illustrated in Figures 1 and 2? (ii) Do the different numerical schemes provide consistent descriptions of the various terms of the PES? (iii) What terms of the PES (cubic, quartic, one-mode, two-mode, etc.) are the most sensitive to the numerical parameters used in their evaluation?

Four systems are considered: two molecular (water, H_2O, and methane, CH_4) and two extended crystalline materials (MgH_2 magnesium hydride and low-temperature proton-ordered phase of water ice, Ice-XI) Figure 5. For the two molecular systems,
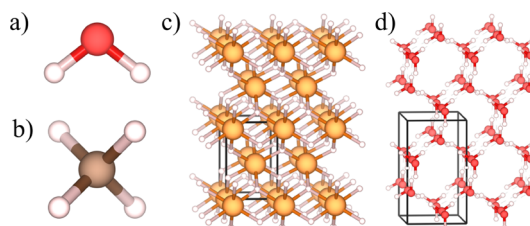

Figure 5. Atomic structure of the four systems used in this study: (a) water molecule, H_2O, (b) methane molecule, CH_4, (c) crystal of magnesium hydride, MgH_2, and (d) low-temperature, proton-ordered phase of water ice, Ice-XI.

water and methane, a 6-31G* basis set is used, and all their vibration modes are considered (i.e., $M = 3$ for water and $M = 9$ for methane in the construction of the PES). Within the 2M4T representation of the potential, this corresponds to a total number N_η of cubic and quartic force constants of 21 and 198, respectively. MgH_2 is a tetragonal crystal with the rutile structure (space group $P4_2/mnm$) and with 6 atoms/cell. Ten vibration modes ($M = 10$) are considered in the definition of the PES, which were selected so as to span the whole spectrum of lattice vibrations (the smallest having a vibration frequency of 210 cm^{-1} and the largest of 1295 cm^{-1}). In its 2M4T representation, the PES consists of $N_\eta = 245$ cubic and quartic force constants. An 8-511G* basis set is used,[62] in combination with a shrinking

factor of 8, which corresponds to sampling over 75 symmetry-irreducible **k**-points in the first Brillouin zone. Ice-XI belongs to the orthorhombic $Cmc2_1$ space group and contains 12 atoms/cell (four water molecules). A subset of 12 vibration modes ($M = 12$) is identified in the definition of the PES (not the full set of modes to reduce the computational time), which were chosen to span the whole spectrum of lattice vibrations (the smallest having a vibration frequency of 274 cm^{-1} and the largest of 3226 cm^{-1}). More specifically, these 12 modes were selected so as to cover the different types of lattice vibrations of ice: four "translations", three "librations", two "bending", and three "stretching" modes. In the 2M4T representation, in this case, the PES has $N_\eta = 354$ force constants. An 8-411G* basis set is used,[63] in combination with a shrinking factor of 4, which corresponds to sampling over 21 symmetry-irreducible **k**-points in the first Brillouin zone. All calculations are performed with the B3LYP hybrid functional of the density functional theory. The effect of the adopted basis set and DFT functional on the description of the anharmonic vibrational states of these systems are explicitly investigated and discussed in Part II of our study.

We start by investigating the numerical stability of the four schemes illustrated in Section IIB for the evaluation of the high-order terms of the PES. In particular, we address their stability with respect to the amplitude I of the explored range of atomic displacements in the definition of the 2D grids of points in Figures 1 and 2. As discussed in Section IIB6, the step size h and displacement range amplitude I are given in units of the "'classical amplitude'" of the harmonic oscillator. For each scheme and for each investigated system, the values of the force constants of the 2M4T representation of the PES obtained with $I = 0.9$ (see Figure 1 for a graphical definition of I) are arbitrarily chosen as an internal reference. In order to discuss the impact of I on the computed values for the force constants, the following mean absolute deviation $|\bar{\Delta}|^I$ (in %) is defined for each scheme and system considered

$$|\bar{\Delta}|^I = \frac{1}{N_\eta'} \sum_{x=1}^{N_\eta'} \frac{|\eta_x^I - \eta_x^{I=0.9}|}{|\eta_x^{I=0.9}|} \times 100 \tag{36}$$

where the sum runs over the N_η' force constants of the PES whose absolute value is larger than 30 cm^{-1} and where η_x^I are the values of force constants computed by exploring an amplitude I in the definition of the grids as in Figure 1.

The mean absolute deviation introduced in eq 36 is reported in Figure 6 as a function of I, where each panel corresponds to a different scheme in the evaluation of the PES. For each scheme, the four systems introduced above are considered. All schemes are relatively stable with respect to the explored range of atomic displacements, with specific features listed below: (i) The two schemes based only on the energy (Schemes 1 and 2) tend to be less stable than the others when small values of I are used in the definition of the grid (indeed, when small atomic displacements from the equilibrium nuclear configuration are performed, the energy alone is unable to fully catch the high-order terms of the PES). (ii) The two EGH schemes that use both energy and forces computed at displaced configurations (Schemes 3 and 4) are characterized by a higher numerical stability with respect to I. (iii) For each scheme, the gray area in Figure 6 highlights the range of displacements within which the scheme shows deviations below 3% for all systems and can be used as an eye-guide (Schemes 3 and 4 are characterized by a wider gray area of stability than Schemes 1 and 2). (iv) The description of the PES of methane and Ice-XI (red and green lines, respectively) turns
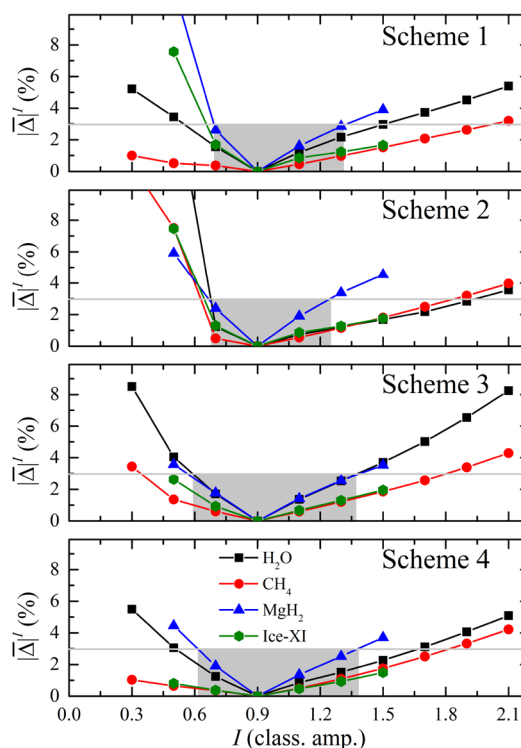

Figure 6. Numerical stability of the four schemes discussed in Section IIB for the description of the PES (in its 2M4T representation) with respect to the amplitude I of the explored range of atomic displacements in the definition of the 2D grid of points. See Figure 1 for a graphical definition of the grids and of I. For each scheme, four systems are considered: molecules of water and methane and the MgH$_2$ crystal and Ice-XI crystal. The plots report the mean absolute deviation $|\bar{\Delta}|^I$ (in %) of the computed high-order (cubic and quartic) force constants with respect to a reference calculation at $I = 0.9$. See eq 36 for an exact definition of this quantity. For each scheme, the gray area highlights the range of displacements within which the scheme shows deviations below 3% for all systems.

out to be extremely stable with respect to the explored interval I for all methods, while the description of the PES of the water molecule and the MgH$_2$ crystal is more sensitive to I.

In Figure 6, we analyzed the overall numerical stability of the different schemes in the description of the 2M4T representation of the PES. Different types of force constants (cubic versus quartic, one-mode versus two-mode) are characterized by different numerical stabilities. We illustrate this aspect by referring to Figure 7, where the numerical stability of the four schemes in the description of the different terms of the PES of Ice-XI is reported as a function of I. Results are shown only for Ice-XI as the considerations to be made below are common to all investigated systems. For each scheme, four sets of force constants are considered: cubic 1M (η_{iii} for all modes), quartic 1M (η_{iiii} for all modes), cubic 2M (η_{iij} and η_{ijj} for all pairs of modes with $i < j$), and quartic 2M (η_{iiij}, η_{ijjj} and η_{iijj} for all pairs of modes with $i < j$). Figure 7 reports mean absolute deviations $|\bar{\Delta}|^I$ (in %) with respect to reference calculations at $I = 0.9$. The four panels in the figure have different vertical scales so that a horizontal gray line is drown at a 3% deviation as an eye-guide to help reading relative values. We see that, overall, as already discussed from Figure 6, Scheme 4 is the most numerically stable, followed by Scheme 3, while the two schemes based only on the energy (Schemes 2 and 1) are less stable. In particular we
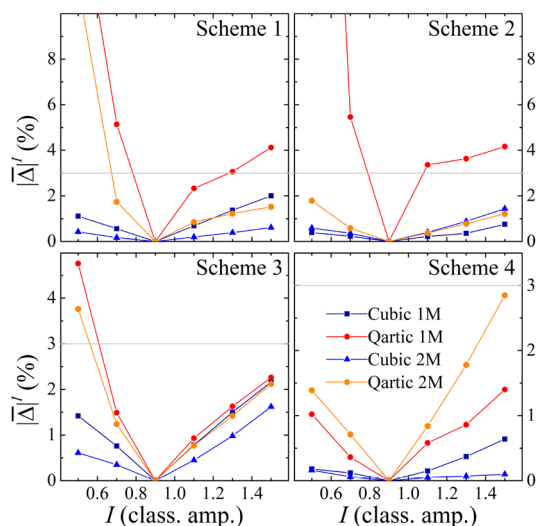
Figure 7. Numerical stability of the four schemes discussed in Section IIB for the description of the PES (in its 2M4T representation) of Ice-XI with respect to the amplitude I of the explored range of atomic displacements in the definition of the 2D grid of points. See Figure 1 for a graphical definition of the grids and of I. For each scheme, four sets of force constants are considered: cubic 1M (η_{iii} for all modes), quartic 1M (η_{iiii} for all modes), cubic 2M (η_{iij} and η_{ijj} for all pairs of modes with $i < j$), and quartic 2M (η_{iiij}, η_{ijjj}, and η_{iijj} for all pairs of modes with $i < j$). The plots report the mean absolute deviation $|\bar{\Delta}|^I$ (in %) of the computed force constants with respect to a reference calculation at $I = 0.9$. Plots have different vertical scales so that a horizontal gray line is drown at a 3% deviation as an eye-guide.

observe that, while cubic force constants (dark and light blue lines for one-mode and two-mode, respectively) are very stable in all the four schemes (with deviations always below 2% in the whole explored range for I), quartic force constants are way more sensitive to the adopted displacement amplitude I when only the energy is computed at displaced nuclear configurations. This becomes particularly critical for the one-mode η_{iiii} terms that show the largest deviations for Schemes 1 and 2.

So far, we have discussed the internal stability of each scheme with respect to the amplitude of the explored range of atomic displacements. Now, we want to investigate whether or not the different numerical schemes provide a consistent description of the PES. To do so, we fix the value of I to 0.9, we take Scheme 4 as an arbitrary reference (this scheme is also expected to be the most accurate as it uses information on the forces at many displaced configurations), and we compute the following mean absolute deviation of the computed force constants with respect to the other schemes $S = 1, 2, 3$

$$|\bar{\Delta}|^S = \frac{1}{N_\eta{}'} \sum_{x=1}^{N_\eta{}'} \frac{|\eta_x^S - \eta_x^{S=4}|}{|\eta_x^{S=4}|} \times 100 \tag{37}$$

This quantity is reported in Table 1, where we can see the following: (i) Different schemes provide a very consistent description of the PES for all systems with deviations larger than 3% only in two cases (both referring to the MgH$_2$ system). (ii) The EGH Scheme 3 provides a description of the PES that is very close to that obtained with the more expensive Scheme 4, with deviations always below 3% for all systems. (iii) Methane turns out to be the most stable system (with deviations among different schemes never exceeding 1.1%), followed by Ice-XI (with deviations never exceeding 1.8%), water, and MgH$_2$.

Table 1. Mean Absolute Deviation $|\bar{\Delta}|^S$ (in %) of Force Constants in 2M4T Representation of PES as Computed with Schemes 1, 2, and 3 ($S = 1, 2, 3$) with Respect to Scheme 4[a]

	Molecules		Solids	
Scheme	H$_2$O	CH$_4$	MgH$_2$	Ice-XI
1	2.6	0.5	5.6	1.8
2	1.5	0.7	3.3	1.4
3	2.5	1.1	2.9	1.6

[a]Calculations are performed with $I = 0.9$ in all cases. Values are given for each scheme for the four systems here considered.

Very similar results (not shown) are obtained for any values of $0.7 \leq I \leq 1.3$. These results are very encouraging as they overall confirm the possibility of getting a stable and reliable description of the high-order anharmonic terms of the PES with the numerical schemes presented in Section IIB. In particular, the EGH Scheme 3 (the one characterized by the lowest computational cost, as documented in Figure 4) is found to be very stable with respect to I and at the same time to provide very consistent values with respect to the most accurate Scheme 4.

IV. CONCLUSIONS AND PERSPECTIVES

Formal and computational aspects related to the description of high-order anharmonic terms (cubic and quartic) of the Born−Oppenheimer potential energy surface (PES) of solids, as obtained from DFT calculations, have been presented. The PES is here truncated after the fourth order and in such a way to contain all one-mode, two-mode, and three-mode terms. Four different numerical approaches (as implemented in the CRYSTAL program), based on a grid representation of the PES in the basis of harmonic normal coordinates, have been illustrated. Two simple molecular systems (water, H$_2$O, and methane, CH$_4$) and two solids (the low-temperature proton-ordered phase of water ice, Ice-XI, and magnesium hydride, MgH$_2$) have been used to test the different methods in terms of numerical stability, accuracy, and computational efficiency.

All methods are found to be sufficiently stable with respect to the explored range of atomic displacements and to provide a consistent description of the different terms of the PES. This is particularly so for cubic terms while quartic terms, and in particular one-mode ones, are more sensitive to the step size used in the definition of the grid. We have identified one promising method (the "'two-point EGH'" scheme) that ensures a good numerical stability and, at the same time, is characterized by a reduced computational cost. It is a finite-difference method working on a minimal grid of points, which uses both the energy and forces computed at selected nuclear configurations.

As a future development, we plan on exploiting the point-symmetry of the lattice in the evaluation of the anharmonic terms of the PES, which is expected to drastically reduce the computational cost of this step of anharmonic calculations. In Part II,[58] we present formal and computational aspects of the VSCF and VCI methods to compute anharmonic vibrational states of solids from the representation of the PES illustrated in the present paper (Part I).

■ AUTHOR INFORMATION

Corresponding Author
*E-mail: alessandro.erba@unito.it.
ORCID
Alessandro Erba: 0000-0002-2986-4254

Jefferson Maul: 0000-0002-4920-1001
Roberto Dovesi: 0000-0002-4657-9439

Notes

The authors declare no competing financial interest.

■ REFERENCES

(1) Born, M.; Huang, K. *Dynamical Theory of Crystal Lattices*; Clarendon Press, 1954.

(2) Hill, T. L. *An Introduction to Statistical Thermodynamics*; Dover Publications, Inc., 1986.

(3) *Infrared and Raman Spectroscopy: Methods and Applications*; John Wiley & Sons, Ltd, 2008.

(4) Squires, G. L. *Introduction to the Theory of Thermal Neutron Scattering*; Cambridge University Press, 2012.

(5) Maradudin, A. A.; Montroll, E. W.; Weiss, G. H. *Theory of Lattice Dynamics in The Harmonic Approximation*; Academic Press: New York, 1963; Vol. 3.

(6) Baroni, S.; de Gironcoli, S.; Dal Corso, A.; Giannozzi, P. Phonons and related crystal properties from density-functional perturbation theory. *Rev. Mod. Phys.* 2001, 73, 515.

(7) Togo, A.; Tanaka, I. First Principles Phonon Calculations in Materials Science. *Scr. Mater.* 2015, 108, 1−5.

(8) Pascale, F.; Zicovich-Wilson, C. M.; López Gejo, F.; Civalleri, B.; Orlando, R.; Dovesi, R. The calculation of the vibrational frequencies of the crystalline compounds and its implementation in the CRYSTAL code. *J. Comput. Chem.* 2004, 25, 888−897.

(9) Gonze, X.; Lee, C. Dynamical matrices, Born effective charges, dielectric permittivity tensors, and interatomic force constants from density-functional perturbation theory. *Phys. Rev. B: Condens. Matter Mater. Phys.* 1997, 55, 10355.

(10) Maul, J.; Erba, A.; Santos, I. M. G.; Sambrano, J. R.; Dovesi, R. Silico Infrared and Raman Spectroscopy Under Pressure: The Case of CaSnO₃ Perovskite. *J. Chem. Phys.* 2015, 142, 014505.

(11) Zhang, W.; Maul, J.; Vulpe, D.; Moghadam, P. Z.; Fairen-Jimenez, D.; Mittleman, D. M.; Zeitler, J. A.; Erba, A.; Ruggiero, M. T. Probing the Mechanochemistry of Metal−Organic Frameworks with Low-Frequency Vibrational Spectroscopy. *J. Phys. Chem. C* 2018, 122, 27442−27450.

(12) Woutersen, S.; Emmerichs, U.; Nienhuys, H.-K.; Bakker, H. J. Anomalous Temperature Dependence of Vibrational Lifetimes in Water and Ice. *Phys. Rev. Lett.* 1998, 81, 1106−1109.

(13) Putrino, A.; Parrinello, M. Anharmonic Raman Spectra in High-Pressure Ice from Ab Initio Simulations. *Phys. Rev. Lett.* 2002, 88, 176401.

(14) Katayama, I.; Aoki, H.; Takeda, J.; Shimosato, H.; Ashida, M.; Kinjo, R.; Kawayama, I.; Tonouchi, M.; Nagai, M.; Tanaka, K. Ferroelectric Soft Mode in a SrTiO₃ Thin Film Impulsively Driven to the Anharmonic Regime Using Intense Picosecond Terahertz Pulses. *Phys. Rev. Lett.* 2012, 108, 097401.

(15) Zhong, W.; Vanderbilt, D.; Rabe, K. M. First-Principles Theory of Ferroelectric Phase Transitions for Perovskites: The Case of BaTiO₃. *Phys. Rev. B: Condens. Matter Mater. Phys.* 1995, 52, 6301−6312.

(16) Cohen, R. E. Origin of Ferroelectricity in Perovskites: The Principal Problems from a Theoretical Perspective. *Ferroelectrics* 1993, 150, 1−12.

(17) Paul, A.; Sun, J.; Perdew, J. P.; Waghmare, U. V. Accuracy of First-Principles Interatomic Interactions and Predictions of Ferroelectric Phase Transitions in Perovskite Oxides: Energy Functional and Effective Hamiltonian. *Phys. Rev. B: Condens. Matter Mater. Phys.* 2017, 95, 054111.

(18) Allen, R. E.; De Wette, F. W. Calculation of Dynamical Surface Properties of Noble-Gas Crystals. I. The Quasiharmonic Approximation. *Phys. Rev.* 1969, 179, 873−886.

(19) Baroni, S.; Giannozzi, P.; Isaev, E. Density-Functional Perturbation Theory for Quasi-Harmonic Calculations. *Rev. Mineral. Geochem.* 2010, 71, 39−57.

(20) Erba, A. On combining temperature and pressure effects on structural properties of crystals with standard ab initio techniques. *J. Chem. Phys.* 2014, 141, 124115.

(21) Erba, A.; Shahrokhi, M.; Moradian, R.; Dovesi, R. On How Differently the Quasi-harmonic Approximation Works for Two Isostructural Crystals: Thermal Properties of MgO and CaO. *J. Chem. Phys.* 2015, 142, 044114.

(22) Erba, A.; Maul, J.; Demichelis, R.; Dovesi, R. Assessing Thermochemical Properties of Materials through Ab initio Quantum-mechanical Methods: The Case of α-Al₂O₃. *Phys. Chem. Chem. Phys.* 2015, 17, 11670−11677.

(23) Erba, A.; Maul, J.; De La Pierre, M.; Dovesi, R. Structural and Elastic Anisotropy of Crystals at High Pressure and Temperature from Quantum-mechanical Methods: The Case of Mg₂SiO₄ Forsterite. *J. Chem. Phys.* 2015, 142, 204502.

(24) Erba, A.; Maul, J.; Itou, M.; Dovesi, R.; Sakurai, Y. Anharmonic Thermal Oscillations of the Electron Momentum Distribution in Lithium Fluoride. *Phys. Rev. Lett.* 2015, 115, 117402.

(25) Erba, A.; Maul, J.; Civalleri, B. Thermal Properties of Molecular Crystals through Dispersion-corrected Quasi-harmonic Ab initio Calculations: The Case of Urea. *Chem. Commun.* 2016, 52, 1820−1823.

(26) Destefanis, M.; Ravoux, C.; Cossard, A.; Erba, A. Thermo-Elasticity of Materials from Quasi-Harmonic Calculations. *Minerals* 2019, 9, 16.

(27) Leibfried, G.; Ludwig, W. In *Theory of Anharmonic Effects in Crystals*; Seitz, F., Turnbull, D., Eds.; Solid State Physics; Academic Press, 1961; Vol. 12; pp 275 − 444.

(28) Plakida, N. M.; Siklós, T. Theory of Anharmonic Crystals. I. General Formulation. *Phys. Status Solidi B* 1969, 33, 103−112.

(29) Togo, A.; Chaput, L.; Tanaka, I. Distributions of Phonon Lifetimes in Brillouin Zones. *Phys. Rev. B: Condens. Matter Mater. Phys.* 2015, 91, 094306.

(30) Togo, A.; Tanaka, I. First Principles Phonon Calculations in Materials Science. *Scr. Mater.* 2015, 108, 1−5.

(31) Plata, J. J.; Nath, P.; Usanmaz, D.; Carrete, J.; Toher, C.; de Jong, M.; Asta, M.; Fornari, M.; Nardelli, M. B.; Curtarolo, S. An Efficient and Accurate Framework for Calculating Lattice Thermal Conductivity of Solids: AFLOW-AAPL Automatic Anharmonic Phonon Library. *NPJ Comput. Mater.* 2017, 3, 45.

(32) Skelton, J. M.; Parker, S. C.; Togo, A.; Tanaka, I.; Walsh, A. Thermal Physics of the Lead Chalcogenides PbS, PbSe, and PbTe from First Principles. *Phys. Rev. B: Condens. Matter Mater. Phys.* 2014, 89, 205203.

(33) Whalley, L. D.; Skelton, J. M.; Frost, J. M.; Walsh, A. Phonon Anharmonicity, Lifetimes, and Thermal Transport in CH₃NH₃PbI₃ from Many-body Perturbation Theory. *Phys. Rev. B: Condens. Matter Mater. Phys.* 2016, 94, 220301.

(34) Linnera, J.; Karttunen, A. J. Ab initio Study of The Lattice Thermal Conductivity of Cu₂O Using the Generalized Gradient Approximation and Hybrid Density Functional Methods. *Phys. Rev. B: Condens. Matter Mater. Phys.* 2017, 96, 014304.

(35) Werthamer, N. R. Self-Consistent Phonon Formulation of Anharmonic Lattice Dynamics. *Phys. Rev. B* 1970, 1, 572−581.

(36) Tadano, S.; Tsuneyuki, T. Self-consistent Phonon Calculations of Lattice Dynamical Properties in Cubic SrTiO₃ with First-principles Anharmonic Force Constants. *Phys. Rev. B: Condens. Matter Mater. Phys.* 2015, 92, 054301.

(37) Tadano, T.; Tsuneyuki, S. Quartic Anharmonicity of Rattlers and Its Effect on Lattice Thermal Conductivity of Clathrates from First Principles. *Phys. Rev. Lett.* 2018, 120, 105901.

(38) Zhou, F.; Nielson, W.; Xia, Y.; Ozoliņš, V. Lattice Anharmonicity and Thermal Conductivity from Compressive Sensing of First-Principles Calculations. *Phys. Rev. Lett.* **2014**, *113*, 185501.

(39) Bowman, J. M. The Self-Consistent-Field Approach to Polyatomic Vibrations. *Acc. Chem. Res.* **1986**, *19*, 202−208.

(40) Monserrat, B.; Drummond, N. D.; Needs, R. J. Anharmonic vibrational Properties in Periodic Systems: Energy, Electron-phonon Coupling, and Stress. *Phys. Rev. B: Condens. Matter Mater. Phys.* **2013**, *87*, 144302.

(41) Engel, E. A.; Monserrat, B.; Needs, R. J. Anharmonic Nuclear Motion and the Relative Stability of Hexagonal and Cubic ice. *Phys. Rev. X* **2015**, *5*, 021033.

(42) Prentice, J. C. A.; Needs, R. J. Using Forces to Accelerate First-principles Anharmonic Vibrational Calculations. *Phys. Rev. Materials* **2017**, *1*, 023801.

(43) Souvatzis, P.; Eriksson, O.; Katsnelson, M. I.; Rudin, S. P. Entropy Driven Stabilization of Energetically Unstable Crystal Structures Explained from First Principles Theory. *Phys. Rev. Lett.* **2008**, *100*, 095901.

(44) Errea, I.; Calandra, M.; Mauri, F. Anharmonic Free Energies and Phonon Dispersions from the Stochastic Self-Consistent Harmonic Approximation: Application to Platinum and Palladium Hydrides. *Phys. Rev. B: Condens. Matter Mater. Phys.* **2014**, *89*, 064302.

(45) Parlinski, K. Ab Initio Determination of Anharmonic Phonon Peaks. *Phys. Rev. B: Condens. Matter Mater. Phys.* **2018**, *98*, 054305.

(46) Christiansen, O.; Luis, J. M. Beyond Vibrational Self-Consistent-Field Methods: Benchmark Calculations for the Fundamental Vibrations of Ethylene. *Int. J. Quantum Chem.* **2005**, *104*, 667−680.

(47) Christiansen, O. Vibrational Structure Theory: New Vibrational Wave Function Methods for Calculation of Anharmonic Vibrational Energies and Vibrational Contributions to Molecular Properties. *Phys. Chem. Chem. Phys.* **2007**, *9*, 2942−2953.

(48) Norris, L. S.; Ratner, M. A.; Roitberg, A. E.; Gerber, R. B. M?ller-Plesset perturbation theory applied to vibrational problems. *J. Chem. Phys.* **1996**, *105*, 11261−11267.

(49) Christiansen, O. M?ller-Plesset perturbation theory for vibrational wave functions. *J. Chem. Phys.* **2003**, *119*, 5773−5781.

(50) Christiansen, O. Vibrational Coupled Cluster Theory. *J. Chem. Phys.* **2004**, *120*, 2149−2159.

(51) Bowman, J. M.; Christoffel, K.; Tobin, F. Application of SCF-SI Theory to Vibrational Motion in Polyatomic Molecules. *J. Phys. Chem.* **1979**, *83*, 905−912.

(52) Zaki, K.; Gélizé-Duvignau, M.; Pouchan, C. Ab initio Cl calculations of the anharmonic force field of methylene-imine CH_2NH. *J. Chim. Phys. PCB* **1997**, *94*, 37.

(53) Carbonnière, P.; Dargelos, A.; Pouchan, C. The VCI-P Code: An Iterative Variation−Perturbation Scheme for Efficient Computations of Anharmonic Vibrational Levels and Ir Intensities of Polyatomic Molecules. *Theor. Chem. Acc.* **2010**, *125*, 543−554.

(54) Baraille, I.; Larrieu, C.; Dargelos, A.; Chaillet, M. Calculation of Non-Fundamental IR Frequencies and Intensities at the Anharmonic Level. I. The Overtone, Combination And Difference Bands of Diazomethane, H_2CN_2. *Chem. Phys.* **2001**, *273*, 91−101.

(55) Neff, M.; Rauhut, G. Toward Large Scale Vibrational Configuration Interaction Calculations. *J. Chem. Phys.* **2009**, *131*, 124129.

(56) Chakraborty, A.; Truhlar, D. G.; Bowman, J. M.; Carter, S. Calculation of Converged Rovibrational Energies and Partition Function for Methane Using Vibrational-Rotational Configuration Interaction. *J. Chem. Phys.* **2004**, *121*, 2071−2084.

(57) Rauhut, G. Configuration Selection as a Route Towards Efficient Vibrational Configuration Interaction Calculations. *J. Chem. Phys.* **2007**, *127*, 184109.

(58) Erba, A.; Maul, J.; Ferrabone, M.; Dovesi, R.; Rérat, M.; Carbonnière, P. Anharmonic Vibrational States of Solids from DFT Calculations. Part II: Implementation of the VSCF and VCI Methods. *J. Chem. Theory Comput.* **2019**, na DOI: 10.1021/acs.jctc.9b00294.

(59) Dovesi, R.; Erba, A.; Orlando, R.; Zicovich-Wilson, C. M.; Civalleri, B.; Maschio, L.; Rérat, M.; Casassa, S.; Baima, J.; Salustro, S.; Kirtman, B. Quantum-Mechanical Condensed Matter Simulations with CRYSTAL. *WIREs Comput. Mol. Sci.* **2018**, *8*, No. e1360.

(60) Erba, A.; Baima, J.; Bush, I.; Orlando, R.; Dovesi, R. Large Scale Condensed Matter DFT Simulations: Performance and Capabilities of the Crystal Code. *J. Chem. Theory Comput.* **2017**, *13*, 5019−5027.

(61) Lin, C. Y.; Gilbert, A. T. B.; Gill, P. M. W. *Theor. Chem. Acc.* **2008**, *120*, 23.

(62) Valenzano, L.; Noël, Y.; Orlando, R.; Zicovich-Wilson, C. M.; Ferrero, M.; Dovesi, R. Ab Initio Vibrational Spectra and Dielectric Properties of Carbonates: Magnesite, Calcite and Dolomite. *Theor. Chem. Acc.* **2007**, *117*, 991−1000.

(63) Bredow, T.; Jug, K.; Evarestov, R. A. Electronic and Magnetic Structure of $ScMnO_3$. *Phys. Status Solidi B* **2006**, *243*, R10−R12.